JOURNAL OF PROPULSION AND POWER
Vol. 21, No. 6, November–December 2005

Concentrations of Nitric Oxide in Laminar Counterflow Methane/Air Diffusion Flames

Tsutomu Shimizu* and Forman A. Williams†
University of California at San Diego, La Jolla, California 92093-0411
and
Alessio Frassoldati‡
Politecnico di Milano, 20133 Milan, Italy

Results of nearly 20 different measurements of profiles of concentrations of oxides of nitrogen in steady counterflow methane-air flames are studied and compared with predictions of four different chemical-kinetic mechanisms. The conditions include air-side strain rates between about 10 and 200 s^{-1}, pressures between 1 and 15 atm, air temperatures between about 300 and 560 K, partial premixing of air on the fuel side down to an equivalence ratio of 1.5, and dilution of the fuel with nitrogen down to a fuel mole fraction of 0.25, all for a fuel temperature of about 300 K. Although most of the experimental results were taken from the literature, two new measurements were made, employing a newly devised NO_x-scrubber technique to correct chemiluminescent NO_x-analyzer results for interference from other species, principally hydrocarbons on the fuel side containing two or more carbon atoms. The results show that differences between measured and predicted NO_x concentrations tend to be smaller on the fuel-lean side of the flame than they are on the fuel-rich side, where typical discrepancies reach values on the order of 50%. Whereas the Milan mechanism, the San Diego mechanism, and the Gas Research Institute (GRI) mechanism version 2.11 usually produce reasonable agreement with the experimental data, the newer GRI mechanism version 3.0 tends to overpredict NO_x under most of the conditions investigated. Because the prompt mechanism is the principal source of NO_x in these flames, this might be associated in some way with the tendency of the GRI mechanisms to overpredict acetylene concentrations by about a factor of two, an overprediction that is demonstrated to occur by comparisons with additional experimental data on concentration profiles of intermediate hydrocarbons.

Nomenclature

a = strain rate, s^{-1}
L = separation distance between the exits of the counterflow ducts, cm
P = pressure, atm
T = temperature, K
u = velocity, cm/s
X = mole fraction
ρ = density, kg/m^3
ϕ = equivalence ratio

Subscripts

1 = fuel stream
2 = airstream

I. Introduction

TO help to mitigate air pollution, there is continuing interest in reduction of NO_x emissions from gas burners.[1] Approaches to achieve this goal include special designs of swirl burners[1] and use of radiant tubes,[2] for example. These devices often involve turbulent combustion of nonpremixed or partially premixed fuels in reaction-sheet regimes.[3] Strategies for NO_x reduction under such conditions can be aided by good knowledge of the chemical kinetics of the structures of laminar diffusion flames, including partially premixed diffusion flames. Laminar counterflow diffusion flames afford useful testing grounds for chemical-kinetic predictions of structures of flames of this type. The counterflow configuration simplifies theoretical computations by reducing the problem to one dimension, resulting in a two-point boundary-value problem for a system of ordinary differential equations, and it also lends itself to accurate experimental measurements. A great deal of research has now been completed on the structures of such "flamelets".[4]

In particular, there are now a number of papers in the literature reporting measurements of structures of nonpremixed and partially premixed laminar counterflow methane-air diffusion flames that include NO profiles.[5–10] Because methane is the major component of natural gas, these measurements are relevant to NO_x emissions during the combustion of natural gas in air. The measurements of NO have been made both by chemiluminescent (CL) NO_x-analyzer analysis following gas sampling and by nonintrusive in situ laser-induced fluorescence (LIF). This extensive database can be used to provide fairly robust tests of predictions of different chemical-kinetic mechanisms. Although some such tests are presented in the previous papers, no all-inclusive evaluation has been published that encompasses the full range of conditions for which experimental results have been reported. An objective of the present contribution is to compare predictions of different chemical-kinetic mechanisms with experiment over the complete range available.

The chemical-kinetic mechanisms chosen for comparison here are the versions 2.11 and 3.0 of the mechanism of the Gas Research Institute, the former name of the current Gas Technology Institute, GRI 2.11[§] and GRI 3.0,[§] the mechanism[11,12] developed at

Presented as Paper 2005-144 at the AIAA Aerospace Sciences Meeting and Exhibit, Reno, NV, 10–13 January 2005; received 20 January 2005; revision received 25 April 2005; accepted for publication 27 April 2005.

*Graduate Student, Department of Mechanical and Aerospace Engineering, Center for Energy Research; tsshimizu@ucsd.edu. Student Member AIAA.
†Professor, Department of Mechanical and Aerospace Engineering, Center for Energy Research; faw@ucsd.edu. Fellow AIAA.
‡Postdoctoral Scholar, CMIC Dipartimento di Chimica, Materiali e Chimica, Piazza Leonardo da Vinci 32; alessio.frassoldati@polimi.it.

§Data available online at http://www.me.berkeley.edu/gri_mech/.

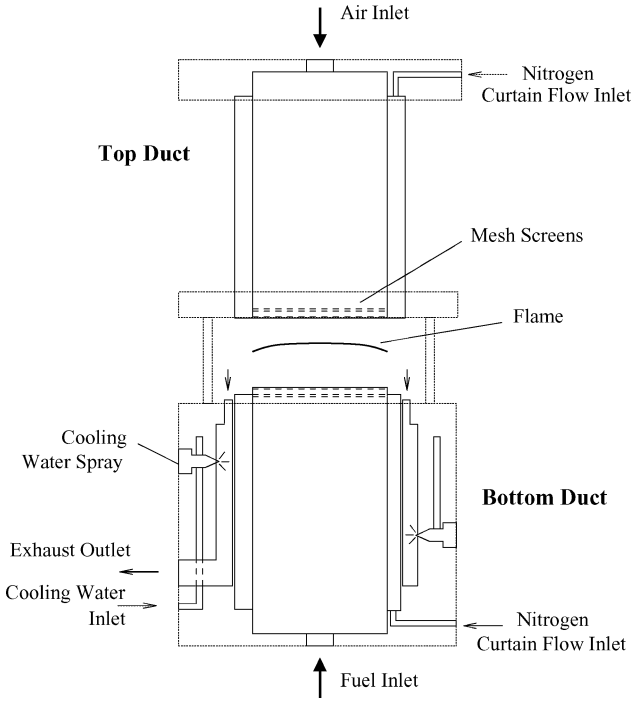

Fig. 1 Schematic illustration of the counterflow burner.

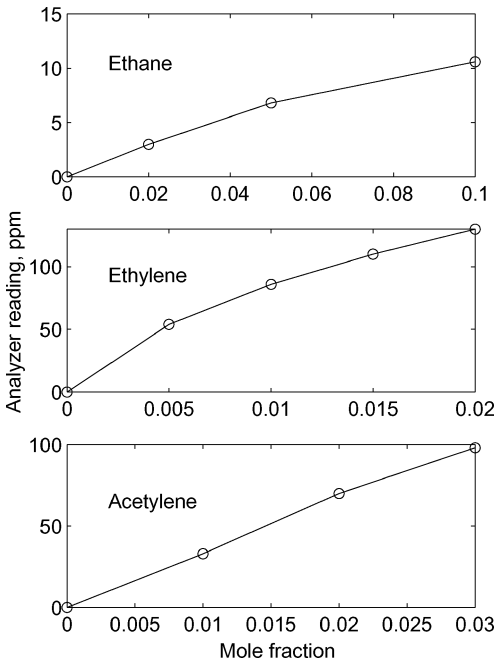

Fig. 2 NO_x-analyzer output readings from ethane, ethylene, and acetylene, as functions of their mole fractions in nitrogen.

Politecnico di Milano and herein for brevity, termed Milan Mech, and the mechanism[13,¶] developed at the University of California, San Diego, called San Diego Mech. GRI mechanisms are selected because of their widespread use in general and because they specifically target natural gas. Besides testing the latest version 3.0 of this mechanism, the previous version 2.11 also is included in the tests because, as will be seen, its predictions are in better agreement with the experimental results under some conditions. Milan Mech is included because it is one of the most extensive and thorough of the current mechanisms; some recent developments in this mechanism will also be indicated. San Diego Mech is the opposite of Milan Mech in the sense that it is designed to be as short as possible and thereby accepts compromises that are not acceptable to other mechanisms; its recent revisions relative to NO also are described. Although the shorter mechanisms capture the main pathways of combustion and NO_x production and destruction, the more complex mechanisms are needed if there is specific interest in particular trace species not fully represented in the simpler mechanisms. By investigating these four mechanisms, we hope to illustrate the range of possible differences in results that can be obtained from different sources.

In addition to the experiments in the literature, results of two new sets of measurements of NO_x profiles are reported. In these new measurements, one set of conditions was selected to correspond to the conditions of one of the flames in the literature, for the purpose of investigating how different the experimental results can be in different laboratories. The other new measurement extends somewhat the range of experimental conditions available in the literature. These new measurements were accomplished by gas sampling and CL analysis. A difficulty with CL analysis is interference from hydrocarbon species, and a new method to correct for this interference is suggested and applied.

II. Experimental Method

Experiments are conducted on methane flames stabilized in the counterflow configuration, introducing methane from the bottom duct and air from the top duct at room temperature.

A schematic illustration of the present burner is shown in Fig. 1. Its details and dimensions are the same as those described by Humer et al.[14] The separation distance between the two ducts was 1.0 cm in the first experiment and 1.5 cm in the second, and the inner diameter of each duct is 2.3 cm. Gas samples are withdrawn from the reaction zone using a quartz microprobe. The probe has a tip with an outer diameter of 0.57 mm and an inner diameter of 0.2 mm. The tip is positioned at a radial distance of about 2 mm off the axis of the ducts to avoid disturbing the flowfield and influencing the concentration profiles in the vicinity of the probe.

The NO_x measurements were obtained using this uncooled quartz microprobe sampling followed by a calibrated NO_x analyzer (model 955, Rosemount Analytical, Inc.). The analyzer measures NO by addition of ozone, leading to the reaction $O_3 + NO \rightarrow O_2 + NO_2^*$, then detecting the chemiluminescent photons emitted by radiative decay of the excited product NO_2^*. To measure total NO_x, NO_2 is chemically reduced to NO before entering the analyzer. The method is very sensitive to NO because the detector is tuned to the photon frequency of deactivation of NO_2^*. Other species present at the same concentration as NO therefore do not affect the reading.

Species present in much larger concentrations can, however, interfere with the NO readings.[15] Various strategies exist for correcting for these interference effects,[**] but unfortunately they all are either inapplicable to our problem or excessively labor intensive. For example, one method is to measure sensitivities of the NO detector to the interfering species, mainly hydrocarbons (some measurements of which are shown in Fig. 2 for our analyzer), then measure the concentrations of these hydrocarbons in the flame by gas chromatographic analysis of the samples withdrawn by the quartz microprobe, and finally use these results to subtract the portions of the signals caused by the interfering species. We have developed a much simpler method for reducing interference in this study.

The new strategy is to make two NO measurements with the analyzer, first a measurement of the complete sample and next a measurement of the sample with NO_x removed. The difference of these two measurements is then the true NO_x measurement. A material is commercially available that removes NO_x, and 18 g of this material, Purafil® Select Chemisorbant Media, are placed in an acrylic tube, which then serves as a NO_x scrubber. Figure 3 illustrates the experimental arrangement employed. After the probe is positioned, NO measurements are made with the flow passing through the bypass

[¶]Data available online at http://maeweb.ucsd.edu/~combustion/cermech/.

[**]Data available online at http://www.epa.gov/airmarkets/monitoring/bias/ [cited Sept. 2004].

Table 1 List of flame conditions of methane-air flames considered in this study

Experiment number	Detection method	X_1	ϕ_1	T_2, K	P, atm	u_1, cm/s	u_2, cm/s	L, cm	a_2, s^{-1}	Reference
1	CL	0.7	——	300	1	15.2	12.5	1.0	50	This study
2	CL	1.0	——	300	1	70	70	1.5	163	This study
3	CL	1.0	——	300	1	70	70	1.5	163	7
4	CL	1.0	——	440	1	70	72.6	1.5	181	7
5	CL	1.0	——	560	1	70	72.6	1.5	192	7
6	LIF	0.25	——	300	1	7	3	2.0	9.5	6
7	LIF	0.25	——	300	1	24	16	2.0	38	6
8	LIF	0.25	——	300	1	38	32	2.0	67	6
9	LIF	0.25	——	300	6	15	15	1.0	58	10
10	LIF	0.25	——	300	8	15	15	1.0	58	10
11	LIF	0.25	——	300	15	15	15	1.0	58	10
12	CL	——	1.5	300	1	23.2	22.5	1.8	50	5
13	CL	——	2.5	300	1	23.6	22.5	1.8	50	5
14	CL	——	3.0	300	1	23.8	22.5	1.8	50	5
15	LIF	——	1.45	300	1	22	18	2.0	39	8
16	LIF	——	1.6	300	1	23	17	2.0	39	8
17	LIF	——	2.0	300	1	23	17	2.0	39	8

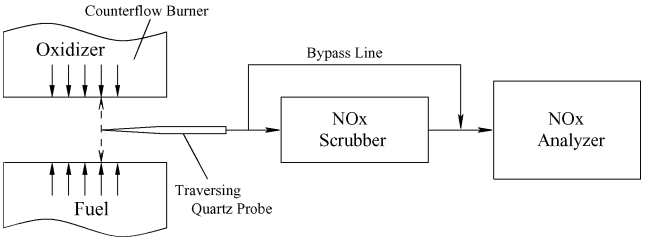

Fig. 3 Schematic illustration of the experimental apparatus for the NO_x-scrubber method.

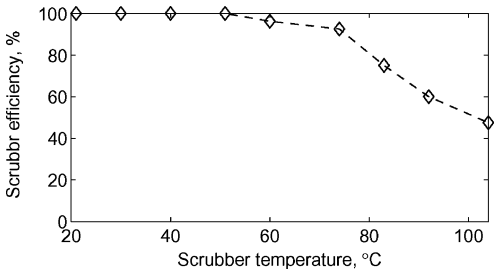

Fig. 4 NO_x-scrubber efficiency as a function of the scrubber temperature.

line, and then the flow is switched to pass through the NO_x scrubber, and NO is measured again. This configuration enables us to measure samples from each line in quick succession at the same probe location in the flame zone.

A complication in these measurements is that this particular NO_x scrubber removes not only NO_x but also various other species as well, including some of the interfering species. To lessen this difficulty, use is made of observed different timescales for response of the analyzer. When any sample is first introduced into the analyzer, because of the low flow rate (slightly less than 0.4 cc/s), it can take the analyzer on the order of 90 s to reach its steady-state response. Similarly, after switching from a NO-nitrogen test gas to air, the signal decays in less than 90 s. Most of the decay times for interfering species were, however, observed to be much longer, on the order of hours. This might possibly be caused by adsorption of these species in feed lines and slow desorption after switching to air. Because of this, when the feed to the analyzer is changed from direct to passage through the scrubber, after 90 s, the signal caused by NO_x has disappeared, but there is still some change in the signal as a result of the interfering species. Measurements therefore are taken 90 s after switching to remove some of the interference effects.

A portion of the signal from the interfering species, however, also decreases during the 90-s period after switching because of their removal by the scrubber. The procedure therefore in practice does not result in a true NO_x measurement but rather in an upper bound for NO_x concentrations. Especially on the fuel side, however, this upper bound is considerably lower than the uncorrected value that would be obtained if the interference effects were neglected. The difference is typically a factor of two, and the correction procedure correctly yields zero NO_x concentrations far on the fuel and air sides of the flame, whereas the uncorrected results do not. The corrections for higher hydrocarbon fuels are larger; for decane flames, fuel-side corrections typically are a factor of 10 (Ref. 16). Although the procedures only provide upper bounds for NO_x concentrations, these bounds are significantly lower than the uncorrected results. The maximum values of NO_x overestimates in methane flames with the correction method employed were reasoned to be no more than 15 ppm and to occur near the NO_x peak and slightly on the fuel side thereof, the errors being much less on the air side. The method would yield much more accurate results if a much more selective NO_x scrubber could be found.

To investigate further whether the present NO_x scrubber can be modified to reduce the extent to which it removes interfering species, its performance was tested at elevated temperatures. Increasing the temperature could reduce the extent to which these other species are removed. For example, water condensation occurs at the lower temperatures, and increasing the temperature can reduce this condensation. The calibration gas (40 ppm NO in N_2) was passed through the scrubber when it was maintained at different temperatures, and the output was delivered to the NO_x analyzer. It was observed that the analyzer began to respond when the temperature exceeded 50°C. Figure 4 shows the scrubber efficiency for NO (one minus the ratio of the reading to the known NO concentration in the calibration gas) as a function of temperature, obtained from these measurements. Because 50°C is insufficient for preventing water condensation and the retention of most interfering species, it was concluded that heating the scrubber is not a viable method to improve its performance.

III. Flames Considered

Table 1 lists the flames considered in the present work. The first two of these are from the experiments just described, and the others are from the literature. In this table, as well as elsewhere in this paper, L is the separation distance between the exits of the counterflow ducts, P denotes pressure, the symbol X_1 represents the mole fraction of fuel (methane at 300 K) in the fuel stream when that stream is a mixture of fuel and nitrogen or pure fuel, ϕ_1 denotes the equivalence ratio of the fuel stream when that stream is a fuel-air mixture, and u_1 is the exit velocity of the gas leaving the fuel duct. The subscript 1 refers always to the fuel stream and 2 to the airstream. The symbol T_2 represents the temperature of the airstream, the exit velocity of the air from the air duct is denoted by

u_2, and the air-side strain rate is a_2 and is given by[17]

$$a_2 = 2u_2/L + (2u_1/L)\sqrt{\rho_1/\rho_2} \quad (1)$$

where ρ denotes density, conditions at the exits of the (axisymmetric) ducts being approximated here as plug flow, leading to rotational flow in the counterflow mixing region. Some of the literature[6,8,10] reports only a global strain rate $(u_1 + u_2)/L$ without giving u_1 and u_2 separately; therefore, in experiments 6–11 and 15–17 of Table 1, values of u_1 and u_2 were chosen to align the location of the calculated [NO] peaks with the reported experimental location. Comparisons are not made with the results of Barlow et al.[9] because these experiments employed a so-called Tsuji burner (fuel injection through a porous horizontal cylinder into an upward flowing irrotational airstream), giving different boundary conditions for which Eq. (1) is not applicable; these experiments, which had ϕ_1 of 2.17 and 3.17, a_2 of 22 and 25 s^{-1}, and fuel temperatures of 323 and 340 K, correspond to conditions that are not very different from those of experiments 13 and 14 of Table 1, and the experimental results are quite similar, so that it seems that nothing new would be gained by including comparisons with these experiments.

IV. Numerical Method and Chemical Kinetics

The OPPDIF code was used to compute the diffusion flame between two opposing ducts. The code is based on a model developed by Kee et al.[18] and is obtained from Reaction Design, Inc. The thermodynamic and transport data used were those on the website for each mechanism. For Milan Mech, the thermodynamic data were taken from the CHEMKIN thermodynamic database[19] or the Burcat[20] database, while the transport data were taken from the CHEMKIN transport database[21] or were estimated by following the procedure proposed by Wang and Frenklach.[22] The radiation option associated with the OPPDIF code was selected for flames 1 and 6 through 17 of Table 1; this takes into account an optically thin radiation model for H_2O and CO_2. Radiation was not included for flames 2 through 5 because of convergence problems, but as a result of the low temperatures and higher strain rates it is not important for these flames, a fact that was verified by calculations both with and without radiation for some other flames. Of the mechanisms considered, GRI 2.11 contains 279 elementary reactions involving 49 chemical species, GRI 3.0 has 325 elementary chemical reactions among 53 species, San Diego Mech includes 214 elementary reactions among 50 species, and Milan Mech contains about 5000 reactions among about 250 species.

Milan Mech has been updated following the recent indications of Miller et al.[23] that the branching ratio of the HCCO + NO reaction, which has two product channels leading to HCNO + CO and HCN + CO_2, respectively, needed revision. The reaction rates, based on quantum chemistry calculations, confirm the dominance of the channel leading to HCNO + CO and modify the value of the branching ratio previously used. The updated model improves the prediction of NO under fuel-rich flame conditions without affecting significantly the good agreement previously obtained.[12] The updated NO_x mechanism also improves the agreement with the measurements of Naik and Laurendeau,[24] especially on the fuel-rich side of the flames where chemical kinetics becomes relevant. These are very hot flames that produce equilibrium NO in the main reaction zone and therefore were not addressed in the present study.

The NO_x portion of San Diego Mech was augmented to account for the step HCCO + NO → HCNO + CO, indicated by Nishioka et al.[25] and by Blevins and Gore[26] to be of some importance under certain conditions. In efforts to keep the mechanism short, however, HCNO is not included in this mechanism. Therefore this step was added, at the reported rate,[§] but with HCNO replaced by the more stable isomer HNCO, under the assumption that isomerization occurs sufficiently rapidly that it is not necessary to retain the intermediary. This replacement has a small but noticeable influence on the predictions, decreasing the predicted NO concentrations in the fuel-rich region by up to 10%.

[§]Data available online at http://www.me.berkeley.edu/gri_mech/.

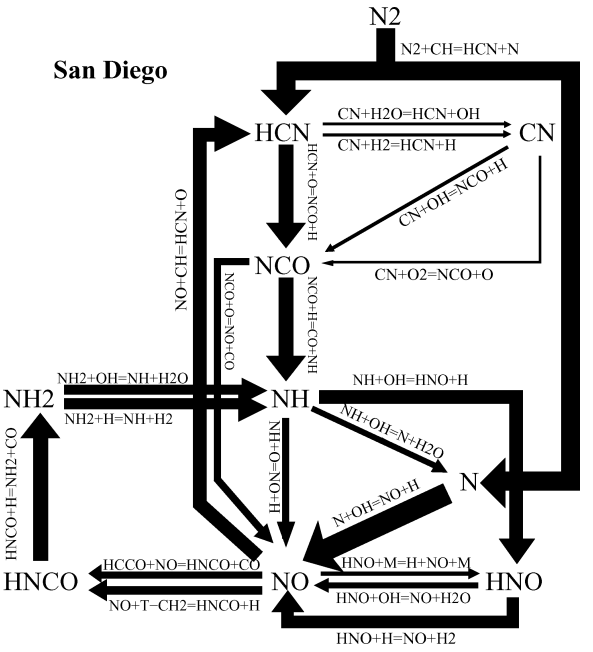

Fig. 5 Reaction-path diagram of San Diego Mech for the undiluted diffusion-flame experiments 2 and 3 of Table 1. Thickness of each arrow is proportional to its reaction rate.

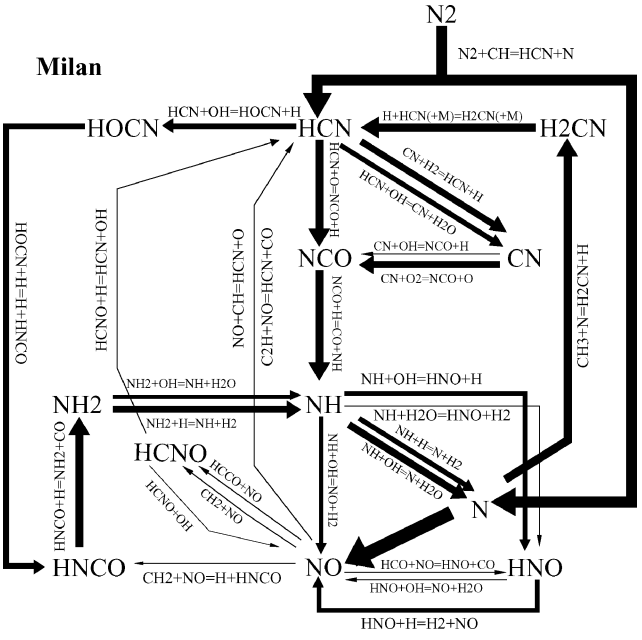

Fig. 6 Reaction-path diagram of Milan Mech for the undiluted diffusion-flame experiments 2 and 3 of Table 1. Thickness of each arrow is proportional to its reaction rate.

It is of interest to exhibit general differences between short and long mechanisms. Reaction-path diagrams for the nitrogen chemistry in flame 2 of Table 1 are shown for San Diego Mech in Fig. 5 and Milan Mech in Fig. 6. In these diagrams, the thickness of the line is proportional to the fraction of the reaction that occurs by the particular path. It can be observed that, in general, there are fewer lines, and the lines are thicker, for San Diego Mech. This occurs because there are many more elementary steps and therefore paths in Milan Mech. Despite this interesting qualitative difference, it will be seen that the differences in NO_x profiles predicted by these two mechanisms are not very great.

V. Results and Discussion

Figure 7 shows the profiles of mole fractions of NO for experiments 1, 2, and 3. The results in experiments 3, 4, and 5 were

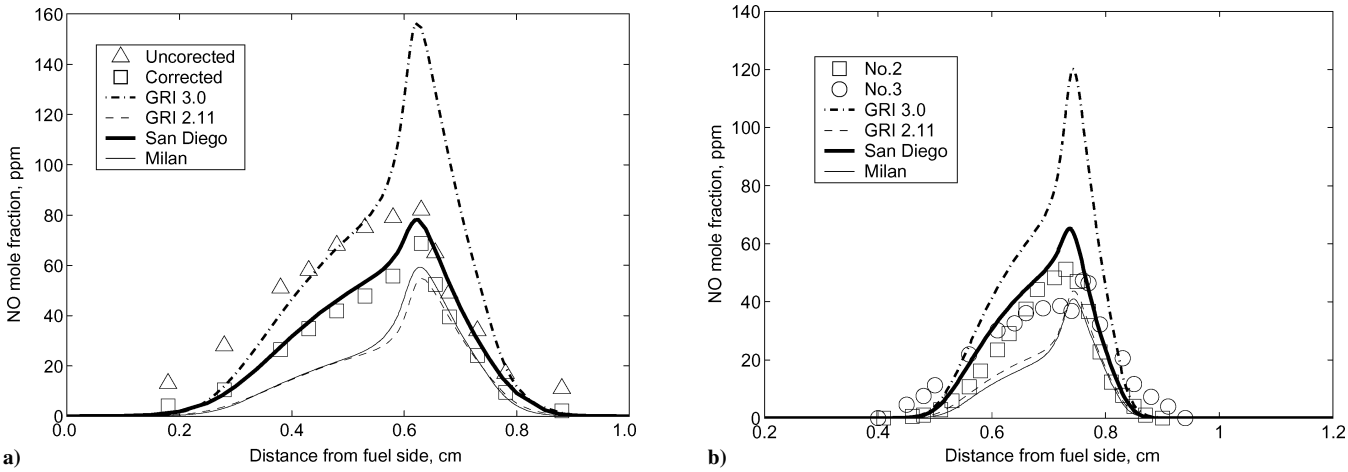

Fig. 7 Profiles of mole fractions of NO for the diffusion-flame a) experiments 1 and b) 2 and 3; symbols are experiments, predictions are from GRI 3.0 (·—·—· curves), GRI 2.11 (- - - - curves), San Diego Mech (—— curves), and Milan Mech (—— curves).

reported on a dry basis, and therefore to better compare those results with others they were corrected to true (wet-basis) mole fractions in the flame, employing the theoretical H_2O profile calculated by San Diego Mech, which is essentially the same as the H_2O profiles calculated by all other mechanisms, in the sense that any resulting differences in corrected NO profiles are well within experimental uncertainty. The left figure shows two sets of experimental results for experiment 1, our uncorrected profiles and our profiles corrected by use of the NO_x scrubber, as described earlier. The correction is seen to be significant, and in this figure all corrected values are estimated to be within 20% of true values, comparable with representative air-side estimates and less than the maximum fuel-side errors discussed earlier. The magnitudes of these corrections for experiment 2 were quite similar to those for experiment 1 everywhere, and therefore only the corrected experimental results are shown in the right figure.

For experiment 1, the predictions of all mechanisms agree with the corrected experimental data, within experimental uncertainty, except those of GRI 3.0, which overpredict NO concentrations by about a factor of two. This increase is a consequence of correcting GRI 2.11, in which the rate constant for the important prompt NO step $CH + N_2 \rightarrow HCN + N$ is too low by slightly more than a factor of two. Because this step is followed by the rapid step $N + O_2 \rightarrow NO + O$, and because HCN also eventually generates NO, an increase in the rate of this step increases the predicted NO concentration roughly proportionally. This overprediction of NO by GRI 3.0 thus suggests that CH concentrations are overpredicted by roughly a factor of two in both GRI 3.0 and GRI 2.11 for experiment 1, although another possibility is that the rates of the so-called reburn processes, shown at the bottom of each diagram in Figs. 5 and 6, that remove NO, are underpredicted. The other two mechanisms both have the correct rate coefficients for the step $CH + N_2 \rightarrow HCN + N$ and therefore can produce their reasonable NO predictions by predicting better CH concentrations. Predictions of Milan Mech are very close to those of GRI 2.11, whereas NO levels predicted by San Diego Mech are somewhat higher. The data fall between the predictions of Milan Mech and San Diego Mech, both of which, however, agree with experiment within experimental error.

These same conclusions follow from similar comparisons seen in the right figure. The main difference between these two figures is the higher strain rate in experiments 2 and 3, which reduces the residence times and thereby decreases NO concentrations somewhat. The two sets of experimental results in this figure are in reasonable agreement, demonstrating acceptable reproducibility of CL measurements in different laboratories. Unfortunately, no LIF measurements have been performed under these conditions, but similar agreements would be anticipated. The curves for experiment 3 are somewhat broader than those for experiment 2, a difference that would occur if the spatial resolution of the sampling probe is poorer in experiment 3, possibly as a consequence of a higher flow rate into the probe.

Figure 8 addresses effects of preheating the airstream because strain-rate differences are small in experiments 3, 4, and 5. Increasing the temperature increases NO mole fractions. The rate of the thermal mechanism, which begins with $O + N_2 \rightarrow NO + N$, is strongly temperature dependent, but under these experimental conditions the prompt mechanism still is dominant, and the smaller increase in the rate of this mechanism with increasing temperature is the main source of the observed NO increase. The NO profiles in the data mirror the shapes in the predictions but are slightly broader at the elevated temperatures, again possibly as a consequence of sampling-probe spatial resolution. Lim et al.[7] also report results of gas-chromatographic measurements of concentration profiles of other species, and the data for acetylene are reproduced in the figure because of its role as precursor of CH. It is seen that the predictions of San Diego Mech are in reasonable agreement with the C_2H_2 data, whereas the other mechanisms overpredict C_2H_2 mole fractions by about a factor of two. This is consistent with the overprediction of NO by GRI 3.0 if C_2H_2 is the primary precursor of CH under these conditions. The overprediction of C_2H_2 by Milan Mech suggests that C_2H_2 plays less of a role in generating CH in that mechanism for the conditions of these experiments.

Figure 9 explores influences of increasing strain rates for highly diluted fuel. The strain rates are necessarily lower in these experiments—6, 7, and 8—to avoid flame extinction. Here the experimental profiles are at least as narrow as the predicted profiles, possibly because of better spatial resolution of the in situ LIF measurement method. The error bars shown here and in later figures are those reported by the authors. The NO levels decrease with increasing strain rate both experimentally and computationally because of the decreased residence time. Because temperatures are low at these high dilutions, the prompt mechanism is dominant. Except for the overpredictions of GRI 3.0, the predictions of all mechanisms are quite close to each other under these conditions and tend to lie within the error bars of the experiments. The agreement with experiment is poorest at the lowest strain rate, which is sufficiently low that buoyancy most likely has an appreciable influence on the experiment, whereas buoyancy is not taken into account in any of the computations. Buoyancy can be expected to skew the data upwards, towards the air duct, and to compress the data somewhat in space, as is seen in the top panel of the figure.

Figure 10 investigates effects of increasing pressure, again at high dilution and by LIF, in experiments 9, 10, and 11. Increasing pressure decreases NO mole fractions in the prompt mechanism by decreasing CH mole fractions. The predictions of the various mechanisms are in reasonable agreement with each other and with experiment at these elevated pressures. Displacements of two of the

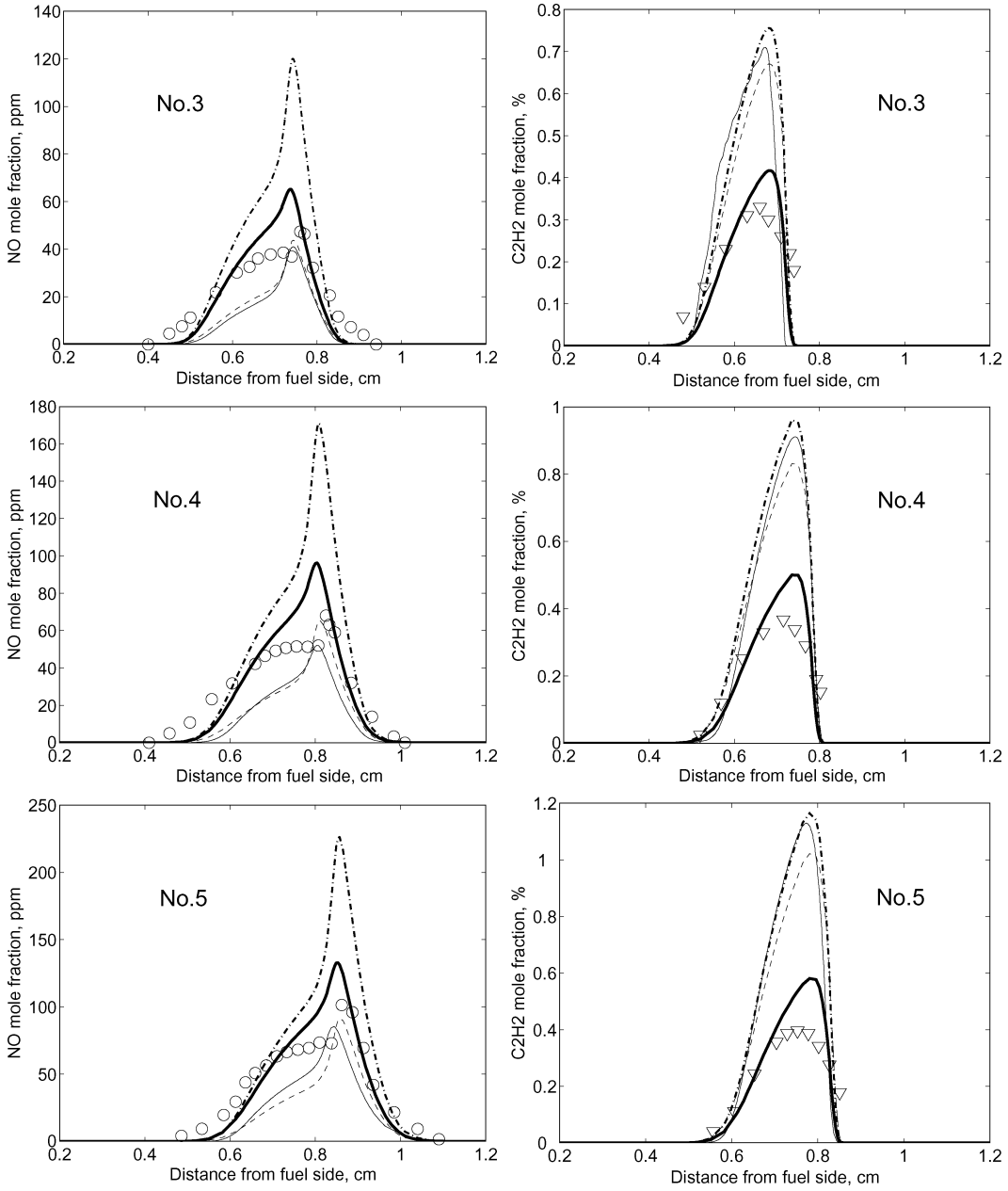

Fig. 8 Profiles of mole fractions of NO (left) and C_2H_2 (right) for the atmospheric-pressure, undiluted diffusion-flame experiments with increasing airstream temperatures, 3 to 5; symbols are experiments, and predictions are from GRI 3.0 (·—·—· curves), GRI 2.11 (- - - - curves), San Diego Mech (—— curves), and Milan Mech (—— curves).

computed peaks, observed in the top two figures, should be ignored because they are an artifact of exit-velocity selections but, especially at the highest pressure, the experimental NO decay on the air side is noticeably slower than predicted by any mechanism, possibly because of buoyant instability in the experiments, a complication that tends to be enhanced at higher pressures. (Computations in which the rate of the step for NO production from N_2O was increased by an order of magnitude failed to produce a significant change in the predicted profile, thereby tending to rule out an effect of the nitrous-oxide mechanism.) Here, GRI 3.0 is as good as or better than the other mechanisms, possibly because it can provide more reasonable predictions of CH at high pressure. In particular, the change in peak [NO] with increasing pressure predicted by GRI 3.0 is in better agreement with experiment than the change predicted by other mechanisms, which exhibit only a small pressure dependence of maximum NO mole fractions at these high pressures.

Figures 11 and 12 address influences of partial premixing, the first (experiments 12, 13, and 14) by CL measurement and the second (experiments 15, 16, and 17) by LIF. The experimental results are similar, although the LIF spatial resolution clearly is better. This similarity supports the view that the two different methods give similar results. In Fig. 12, the present results obtained with GRI 2.11 have somewhat less NO than shown previously[8] with this mechanism, although both sets of computational results fall within the experimental error bars. The CL paper[5] also reports gas-chromatographic measurements of the sum of the concentrations of ethylene and acetylene, for all but the highest equivalence ratio, and these are also shown in Fig. 11 because of their possible relevance to prompt NO. San Diego Mech is seen to agree best with this hydrocarbon data, whereas predictions of the other mechanisms are quite close but somewhat high, although not to the extent seen in Fig. 8. All mechanisms appear to be in reasonable agreement with the data on NO here, although, as before, GRI 3.0 seems to overpredict NO at the higher equivalence ratios, as diffusion-flame conditions are approached. The present predictions of San Diego Mech agree better with experiment than reported previously[5] because of more recent

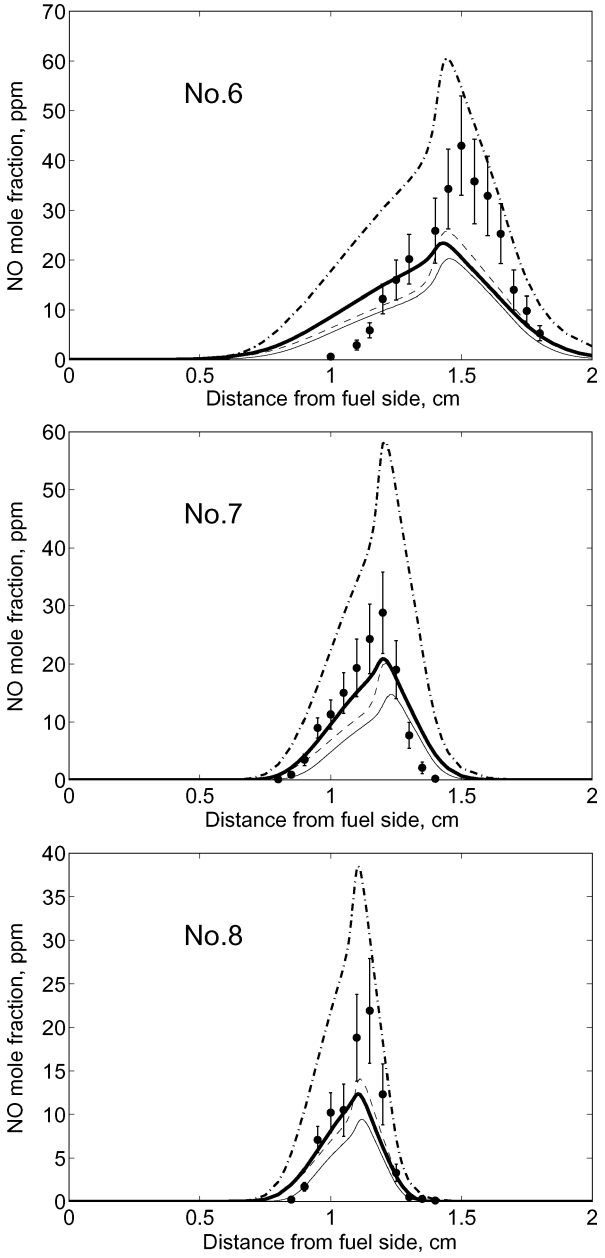

Fig. 9 Profiles of mole fractions of NO for the atmospheric-pressure, highly diluted diffusion-flame experiments with increasing strain rates, 6 to 8; symbols are experiments, and predictions are from GRI 3.0 (·—·—· curves), GRI 2.11 (- - - - curves), San Diego Mech (—— curves), and Milan Mech (—— curves).

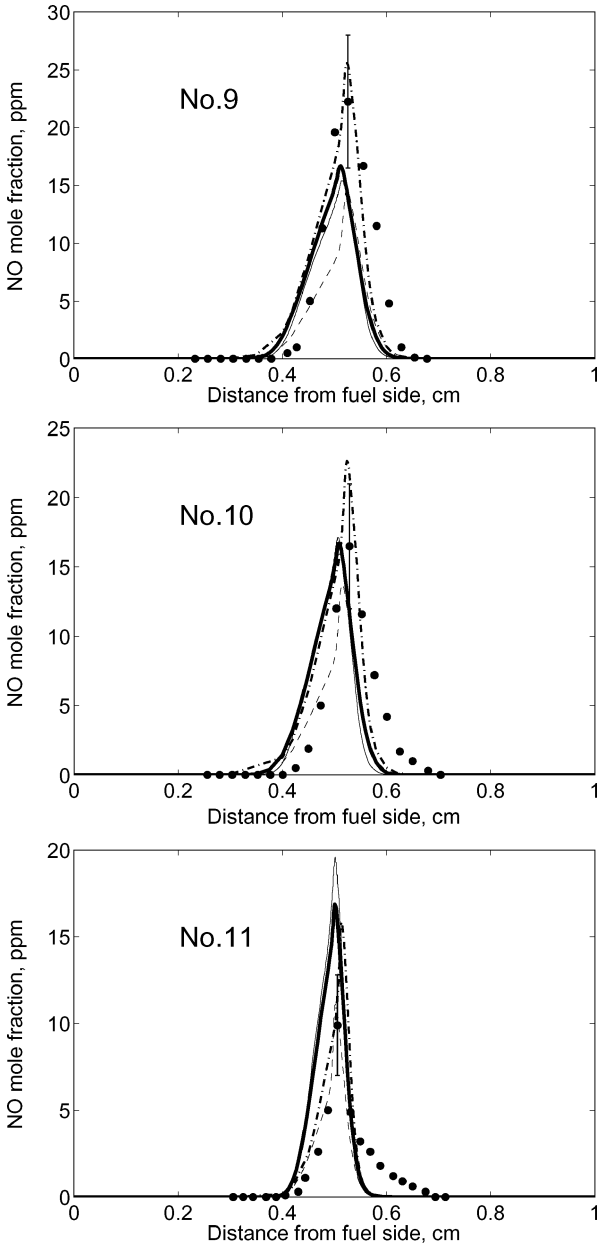

Fig. 10 Profiles of mole fractions of NO for the highly diluted diffusion-flame experiments with increasing pressure, 9 to 11; symbols are experiments, and predictions are from GRI 3.0 (·—·—· curves), GRI 2.11 (- - - - curves), San Diego Mech (—— curves), and Milan Mech (—— curves).

improvements in the mechanism, as discussed previously for NO and as can be obtained from the website[¶] for hydrocarbon species.

VI. Discussion and Conclusions

Because the chemistry of NO production in these flames is dominated by the prompt mechanism, many detailed elementary fuel-chemistry steps leading to the formation of CH are relevant. One path from CH_4 to CH goes directly through CH_3 and CH_2. Another begins with $CH_3 + CH_3 + M \rightarrow C_2H_6 + M$ and proceeds through the stable species C_2H_4 and C_2H_2. Different mechanisms have different contributions from these two path.

Direct measurement of CH is helpful in sorting out the different contributions to the prompt mechanism, and results of one set of measurements of this type, which are quite difficult to perform, have been published.[27] These particular measurements pertain to atmospheric-pressure, diluted, partially premixed flames at the same strain rates and fuel-side equivalence ratios a measurements 15, 16, and 17 of Table 1, as well as to the correspondingly diluted pure diffusion flame. The results of these measurements were found to agree very well with the predictions of GRI 3.0, whereas the CH levels predicted by GRI 2.11 are somewhat low, and those predicted by the San Diego and Milan Mech lie below the data by a factor of two or more and tend to exhibit displacements at the lower equivalence ratios, San Diego Mech to the fuel side and Milan Mech to the air side. The maximum CH concentrations predicted by San Diego Mech are, in fact, lower than those predicted by the GRI mechanisms under all of the conditions of Table 1.

In an overall sense, GRI 3.0 achieves its best agreement with reported experimental results at the higher pressures and higher degrees of dilution and premixing, whereas San Diego Mech exhibits its best agreements at the higher strain rates, higher equivalence ratios and in diffusion flames, although its agreement with the reported[27] CH concentration profiles in highly diluted,

[¶]Data available online at http://maeweb.ucsd.edu/~combustion/cermech/.

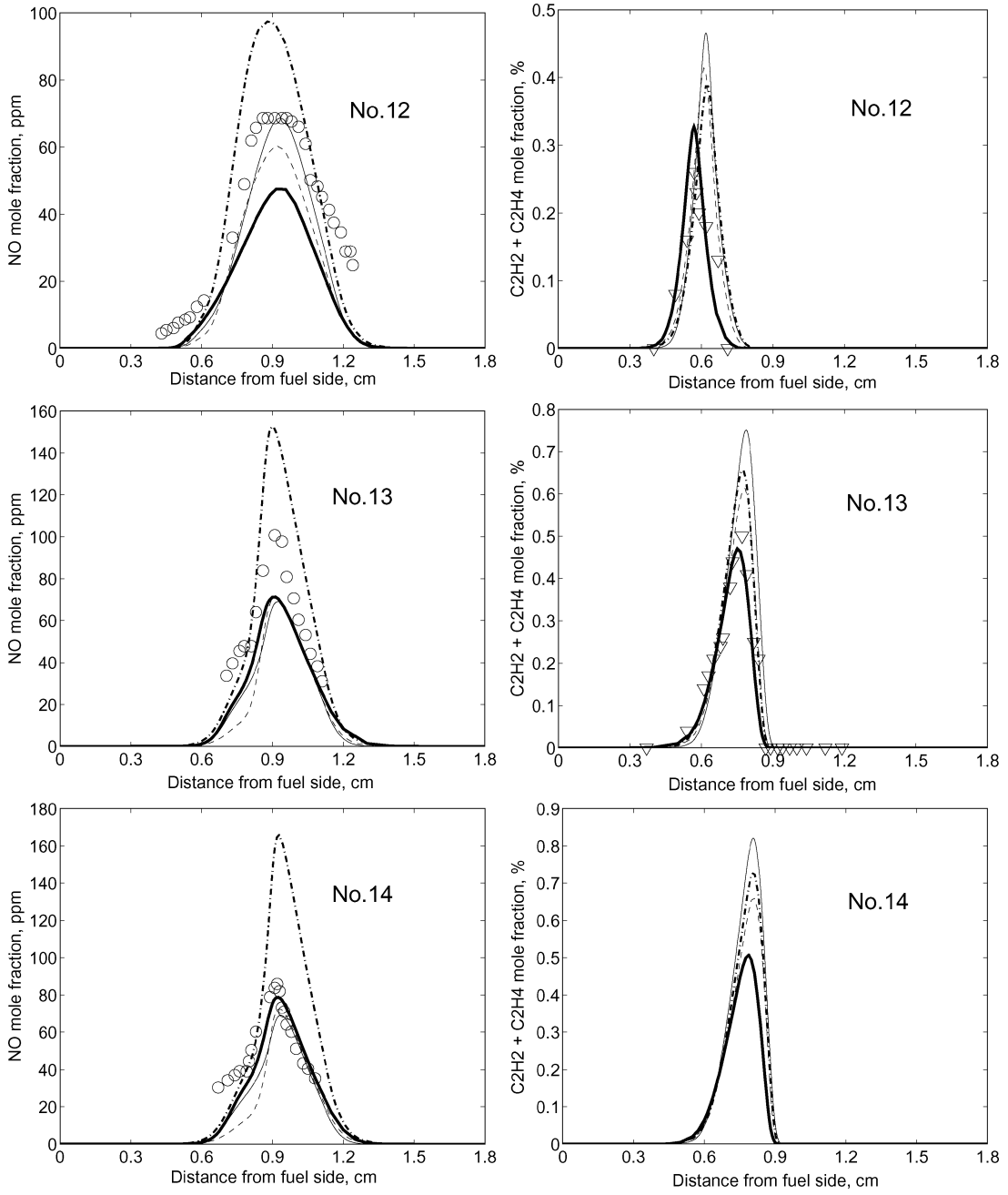

Fig. 11 Profiles of mole fractions of NO (left) and $C_2H_2 + C_2H_4$ (right) for the atmospheric-pressure, partially premixed flames with increasing equivalence ratios (experiments 12 to 14) measured by gas sampling; symbols are experiments, and predictions are from GRI 3.0 (·–·–· curves), GRI 2.11 (- - - - curves), San Diego Mech (—— curves), and Milan Mech (—— curves).

low-strain-rate diffusion flames is poor. The fuel-chemistry predictions of GRI 3.0 and 2.11 are closer to each other than their NO predictions but still differ by as much as 50% in their CH predictions in some cases, whereas the fuel-chemistry predictions of the other two mechanisms tested tend to differ much more. Predicted maximum CH concentrations are appreciably more sensitive to the mechanism employed than are predicted maximum NO concentrations, the former exhibiting differences of more than an order of magnitude in some cases. These observations point towards further studies of the fuel chemistry leading to CH as fruitful lines of investigation for improving capabilities to predict prompt NO_x accurately in methane-air flames.

It can be concluded in general from these comparisons that chemical-kinetic mechanisms that produce reasonable agreement (that is, discrepancies much less than a factor of two) with measured profiles of NO in counterflow methane-air flames are available, under all conditions for which measurements have been made. Predicted variations with air temperature, strain rate, pressure, fuel dilution, and partial premixing also agree with experiments, at least qualitatively. Some mechanisms, however, do not yield very good agreement under some conditions; for example, GRI 3.0 overpredicts NO concentrations, as well as C_2H_2 concentrations, for all existing experiments except those with highly diluted flames at higher pressures, 6 to 15 atm, where it performs as well as or better than other mechanisms. Because the prompt mechanism is the main source of NO in all of the flames for which measurements have been made, the experiments do not test how well the mechanisms can predict thermal NO, although that mechanism is simpler and has better known elementary rate parameters than the prompt mechanism, and most mechanisms have essentially the same rate parameters for the thermal mechanism, so that agreement with experiment would be anticipated when the thermal mechanism is dominant.

There are, however, ranges of conditions for which experiments do not yet exist and for which tests of predictions therefore

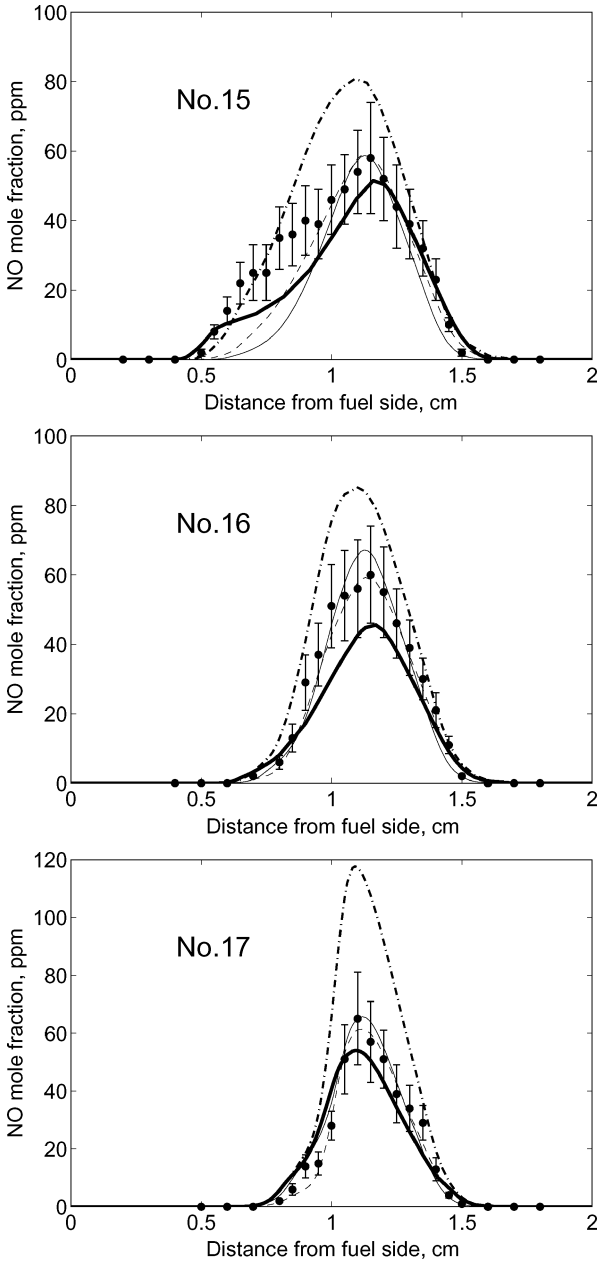

Fig. 12 Profiles of mole fractions of NO for the atmospheric-pressure, partially premixed flames with increasing equivalence ratios (experiments 15 to 17) measured by LIF; symbols are experiments, and predictions are from GRI 3.0 (·—·—· curves), GRI 2.11 (- - - - curves), San Diego Mech (—— curves), and Milan Mech (—— curves).

cannot be made. These conditions include all low-pressure diffusion flames (pressure below 1 atm) and especially high-pressure, high-temperature flames at high strain rates, where the thermal mechanism starts to play a greater role. Because many conditions of practical interest fall within this last category, it would be of interest to try to perform these high-strain-rate experiments. To do so, however, is quite challenging because of the very fine spatial resolution that would be required.

The good agreements that have been found do not imply that the successful chemical-kinetic mechanisms are now correct. Many uncertainties in rate parameters for elementary steps remain in all mechanisms. Further research in improving the chemical-kinetic mechanisms by reducing these uncertainties therefore is warranted.

Acknowledgments

This research was supported by the U.S. National Science Foundation through Grant CTS 0129562. The Rotary Foundation provided partial financial support to T. Shimizu. We would like to thank Reinhard Seiser and Stefan Humer for instructions on use of the counterflow burner and the gas sampling technique and Bruce Thomas for his help in setting up this experiment at University of California at San Diego. We would also like to thank Eliseo Ranzi and Tiziano Faravelli for helpful discussions on chemical-kinetic modeling. We acknowledge Teledyne Advanced Pollution Instrumentation for their advice concerning the use of Purafil® Select Chemisorbant Media to scrub NO_x from sample gases.

References

[1]Spangelo, Ø., Slungaard, T., Engebretsen, T., and Sønju, O. K., "Development of Low NO_x Swirl Burner for Gaseous Fuels," *Proceeding of the Seventh International Conference on Energy for a Clean Environment*, 2003, pp. 110–125; also Spangelo, Ø., "Experimental and Theoretical Studies of a Low NO_x Swirl Burner," Ph.D. Dissertation, Dept. of Energy and Process Engineering, NTWU 2004:78, Norwegian Univ. of Science and Technology, Trondheim, Norway, 2004, Appendix A.

[2]Blevins, L. G., and Gore, J. P., "A Study of Radiant Tube Flame Structure and NO_x Emissions," *Combustion Science and Technology*, Vol. 109, Nos. 1–6, 1995, pp. 255–271.

[3]Williams, F. A., "Some Recent Studies in Turbulent Combustion," *Smart Control of Turbulent Combustion*, Springer-Verlag, Tokyo, 2001, pp. 1–12.

[4]Williams, F. A., "Progress in Knowledge of Flamelet Structure and Extinction," *Progress in Energy and Combustion Science*, Vol. 26, Nos. 4–6, 2000, pp. 657–682.

[5]Li, S. C., and Williams, F. A., "NO_x Formation in Two-Stage Methane-Air Flames," *Combustion and Flame*, Vol. 118, No. 3, 1999, pp. 399–414.

[6]Ravikrishna, R. V., and Laurendeau, N. M., "Laser-Induced Fluorescence Measurements and Modeling of Nitric Oxide in Methane-Air and Ethane-Air Counterflow Diffusion Flames," *Combustion and Flame*, Vol. 120, No. 3, 2000, pp. 372–382.

[7]Lim, J., Gore, J., and Viskanta, R., "A Study of the Effects of Air Preheat on the Structure of Methane/Air Counterflow Diffusion Flames," *Combustion and Flame*, Vol. 121, Nos. 1/2, 2000, pp. 262–274.

[8]Ravikrishna, R. V., and Laurendeau, N. M., "Laser-Induced Fluorescence Measurements and Modeling of Nitric Oxide in Counterflow Partially Premixed Flames," *Combustion and Flame*, Vol. 122, No. 4, 2000, pp. 474–482.

[9]Barlow, R. S., Karpetis, A. N., Frank, J. H., and Chen, J. Y., "Scalar Profiles and NO Formation in Laminar Opposed-Flow Patially-Premixed Methane/Air Flames," *Combustion and Flame*, Vol. 127, No. 3, 2001, pp. 2102–2118.

[10]Ravikrishna, R. V., Naik, S. V., Cooper, C. S., and Laurendeau, N. M., "Quantitative Laser-Induced Fluorescence Measurements and Modeling of Nitric Oxide in High-Pressure (6-15 atm) Counterflow Diffusion Flames," *Combustion Science and Technology*, Vol. 176, No. 1, 2004, pp. 1–21.

[11]Faravelli, T., Frassoldati, A., and Ranzi, E., "Kinetic Modeling of the Interactions Between NO and Hydrocarbons in the Oxidation of Hydrocarbons at Low Temperatures," *Combustion and Flame*, Vol. 132, Nos. 1/2, 2003, pp. 188–207.

[12]Frassoldati, A., Faravelli, T., and Ranzi, E., "Kinetic Modeling of the Interactions Between NO and Hydrocarbons in the Oxidation of Hydrocarbons at High Temperature," *Combustion and Flame*, Vol. 135, Nos. 1/2, 2003, pp. 97–112.

[13]Hewson, J. C., and Bollig, M., "Reduced Mechanisms for NO_x Emissions from Hydrocarbon Diffusion Flames," *Twenty-Sixth Sympsiumm (International) on Combustion*, The Combustion Institute, Pittsburgh, PA, 1996, pp. 2171–2179.

[14]Humer, S., Seiser, R., and Seshadri, K., "Non-Premixed and Premixed Extinction and Autoignition of C2H4, C2H6, C3H6, and C3H8," *Twenty-Ninth Sympsiumm (International) on Combustion*, The Combustion Institute, Pittsburgh, PA, 2002, pp. 1597–1604.

[15]Tidona, R. J., Nizami, A. A., and Cermansky, N. P., "Reducing Interference Effects in the Chemiluminescent Measurement of Nitric Oxides from Combustion Systems," *Journal of Air Pollution Control Association*, Vol. 38, No. 6, 1988, pp. 806–811.

[16]Shimizu, T., "Experimental and Numerical Analysis of Species Profiles and NO Formation in Laminar Counterflow Methane/Air and n-Decane/Air Diffusion Flames," M.S. Thesis, Univ. of California at San Diego, La Jolla, CA, 2005.

[17]Seshadri, K., and Willams, F. A., "Laminar Flow Between Parallel Plates with Injection of a Reactant at High Reynolds Number," *International Journal of Heat and Mass Transfer*, Vol. 21, No. 2, 1978, pp. 251–253.

[18]Kee, R. J., Miller, J. A., Evans, G. H., and Dixon-Lewis, G., "A Computational Model of the Structue and Extinction of Strained, Opposed Flow, Premixed Methane-Air Flames," *Twenty-Second Sympsiumm (International) on Combustion*, The Combustion Institute, Pittsburgh, PA, 1988, pp. 1479–1494.

[19]Kee, R. J., Rupley, F., and Miller, J. A., "The Chemkin Thermodynamic Data Base," Sandia National Lab., Rept. SAND 89-8008, 1989.

[20]Burcat, A., "Third Millennium Ideal Gas and Condensed Phase Thermochemical Database for Combustion," Technion Aerospace Engineering (TAE), Rept. # 867, 2001, URL: http://ftp.technion.ac.il/pub/supported/aetdd/thermodynamics.

[21]Kee, R. J., Dixon-Lewis, G., Warnatz, J., Coltrin, M. E, and Miller, J. A., "The Chemkin Transport Data Base," Sandia Lab., Rept. SAND 86-8246, 1986.

[22]Wang, H., and Frenklach, M., "Transport Properties of Polycyclic Aromatic Hydrocarbons for Flame Modeling," *Combustion and Flame*, Vol. 96, Nos. 1/2, 1994, pp. 163–170.

[23]Miller, J. A., Klippenstein, S. J., and Glarborg, P., "A Kinetic Issue in Reburning: The Fate of HCNO," *Combustion and Flame*, Vol. 135, No. 3, 2003, pp. 357–362.

[24]Naik, S. V., and Laurendeau, N. M., "Quantitative Laser-Saturated Fluorescence Measurement of Nitric Oxide in Counter-Flow Diffusion Flames Under Sooting Oxy-Fuel Conditions," *Combustion and Flame*, Vol. 129, Nos. 1/2, 2002, pp. 112–119.

[25]Nishioka, M., Kondoh, Y., and Takeno, T., "Behavior of Key Reactions on NO Formation in Methane-Air Flames," *Twenty-Sixth Sympsiumm (International) on Combustion*, The Combustion Institute, Pittsburgh, PA, 1996, pp. 2139–2145.

[26]Blevins, L. G., and Gore, J. P., "Computed Structure of Low Strain Rate Partially Premixed CH_4/Air Counterflow Flames: Implications for NO Formation," *Combustion and Flame*, Vol. 116, No. 4, 1999, pp. 546–566.

[27]Naik, S. V., and Laurendeau, N. M., "Measurements of Absolute CH Concentrations by Cavity Ring-Down Spectroscopy and Linear Laser-Induced Fluorescence in Laminar, Counterflow Partially Premixed and Nonpremixed Flames at Atomospheric Pressure," *Applied Optics*, Vol. 43, No. 26, 2004, pp. 5116–5125.